Available online at www.sciencedirect.com

ScienceDirect

journal homepage: www.elsevier.com/locate/he

Two-dimensional numerical simulations of detonation cellular structures in H_2–O_2–Ar mixtures with OpenFOAM®

L.F. Gutiérrez Marcantoni [a,b,*], J. Tamagno [a], S. Elaskar [a,b]

[a] Departamento de Aeronáutica, Facultad de Ciencias Exactas, Físicas y Naturales, Universidad Nacional de Córdoba, Córdoba, Argentina

[b] Instituto de Estudios Avanzados en Ingeniería y Tecnología (IDIT), CONICET – UNC, Argentina

ARTICLE INFO

Article history:
Received 11 February 2017
Received in revised form
20 July 2017
Accepted 27 August 2017
Available online 19 September 2017

Keywords:
Kurganov schemes
OpenFOAM®
Detonation
Cellular structures

ABSTRACT

In the present work, the solver rhoCentralRfFoam, developed using the finite volume framework provided by OpenFOAM®, is employed to perform numerical simulations of two-dimensional detonations. This solver uses the central scheme of Kurganov, Noelle, and Petrova for dealing with convective terms. Also, the detailed kinetic model for hydrogen oxidation of Marinov, Westbrook, and Pitz was used for properly defining chemically induced source terms, and the semi-implicit Bulirsh Stöer (SIBS) method was employed for solving the stiff ODE system required to compute the species' rates. The present study intends to investigate the solver's capability for computing cellular structures, which develop when non-planar detonations are propagating in confined mixtures. Interactions between waves, resulting from several ignition points, are used as perturbation sources for the onset of cellular structures. Numerical simulations allowed us to identify a well-shaped cellular structure and other different structures that are not clearly defined, close to the ignition sources. However, after extending the computational domain, convergence towards a unique cellular pattern is attained. Such cellular pattern compares with most of the available data. Also, in order to improve the presentation of cellular structures and their dynamic behavior, a numerical *schlieren* technique is utilized for some flow variables (e.g. vorticity and density).

Introduction

Essentially, detonations front shapes are spatially unstable. Moreover, they become discontinuous due to the existence of transverse shocks obliquely propagating to the front, generating shock-shock type interactions. As a result of these interactions, triple point configurations resembling the scales of a fish are built, and are identified as cellular structures [1]. These structures involve interactions of an incident shock, a transverse wave and a Mach stem. Weak and strong types of such structures have been observed in experiments, all conditioned by the strength of transverse waves. Basically, the more reactive the mixture is, the smaller their cells are. Therefore, the use of hydrogen-oxygen mixtures diluted with argon has become a usual practice for obtaining suitable cellular patterns for research [2,3].

* *Corresponding author*. Departamento de Aeronáutica, Facultad de Ciencias Exactas, Físicas y Naturales, Universidad Nacional de Córdoba, Av. Vélez Sarsfield 1611, Córdoba, Argentina.
E-mail addresses: luisgutierrezmarcantoni@conicet.gov.ar, lfgmarcantoni@gmail.com (L.F. Gutiérrez Marcantoni).
http://dx.doi.org/10.1016/j.ijhydene.2017.08.188

Moreover, in order to study cellular structures and to unveil details that cannot be easily identified in experiments, numerical simulations have been increasingly employed [2–8]. Sharpe [9] postulated that an adequate spatial resolution is absolutely vital, and in addition, Hu [10] claims that the use of simplified chemical models could not have included some typical features of complex chain-branching reaction processes. Therefore, for obtaining a proper numerical simulation of detonation cellular structures, a high-resolution mesh and a kinetic model offering a good representation of chain-branching processes are both needed. Any detailed numerical simulation of detonation processes can be an expensive computational task, as it involves resolving a large number of coupled unsteady transport equations and a large stiff system of ordinary differential equations (ODEs). Due to the unsteady nature of detonation processes, the numerical approach must be properly selected. Implicit numerical methods, although theoretically unconditionally stable, are not appropriate for detonation simulations. This is because cumulative numerical damping errors may strongly affect the obtained time-dependent solutions [11]. Therefore, an explicit numerical technique based on the use of fractional steps is preferred. Then, we employed an algorithm with this methodology for simulating detonations in the $2H_2 : O_2 : 7Ar$ combustible mixture. Moreover, in order to ensure an adequate mesh resolution, a procedure based on chemical induction time is utilized. The hydrogen oxidation can be modeled at different levels of detail, from simple mechanisms of few species and reactions up to very detailed ones. When the combustion is controlled by the mixing process, either an equilibrium model or one with simple kinetics may be useful [12–14]. However, this is not the case in detonations, as they are primarily controlled by rates. In previous planar detonation studies performed with H_2-Air mixtures, three different chemical kinetics were taken into consideration: Jachimowski 1988 (J1988) [15], Jachimowski 1992 (J1992) [16] and Marinov 1996 (M1996) [17]. Both Jachimowski's models use 13 species and 33 reactions, and Marinov uses 9 species and 25 reactions. All results obtained with rhoCentralRfFoam solver have been compared to one another for assessing the impact of chemical kinetics modeling. In addition, to verify the code's behavior of the rhoCentralRfFoam solver, typical results (pressure, temperature, density, water mass fraction) were compared with the computed profiles using the FlowTwo code. FlowTwo is a genuine 1D solver, which uses a point implicit time integration technique and a second order Harten-Yee TVD scheme [18–21]. The flow equations in these two codes are further solved using finite volume schemes. Both have shown that results produced using the J1988 chemical model substantially differ from the other two models, while results obtained using J1992 and M1996 are in good agreement. Subsequent to performing simulations with several equivalence ratios of the combustible mixture (H_2–Air), detonation velocities were compared with Chapman-Jouguet (CJ) equilibrium calculations. Again, J1992 and M1996 models predictions are in good agreement with CJ's values, however, the J1988 model predictions do not correlate correctly with those values. It was concluded that be best results are provided by J1992 and M1996 models, but Marinov achieves it with fewer species and reactions. Therefore, in all simulations, Marinov's model shall be used. To further prove which of the above kinetic models is the most convenient, we compared the time evolution of temperature in burning mixtures (starting from given initial values) with reference values provided by CHEMKIN® [22]. From the results of testing the three kinetic models, we concluded that Marinov's model was the best. Consequently, it was also utilized to define induction times (that is, the necessary time to build a radical population capable of promoting ignition of the combustible mixture). These induction times are vital to ensure a proper grid resolution in the computational domain. Detailed information on these previous studies can be found in Refs. [23,24].

The solver rhoCentralRfFoam [23,24], built on the finite volume data structure and libraries provided by OpenFOAM® has been used in all numerical simulations performed here. This solver can be considered as an improvement of rhoCentralFoam, which was originally used in high-speed flows without reactions [25,26], and later, also applied to some high-speed reactive problems [27–30]. However, in this context, there are no numerical simulations describing cellular structures formation in detonating mixtures. It is worth noting that discrete convective terms are evaluated using the second order central-upwind scheme of Kurganov, Noelle and Petrova (KNP) [31], because it has been widely proved that it delivers accurate results with less computational costs, regardless of the particular chemical problem it has been applied to [25,32–36].

This study has two primary purposes – firstly, the verification of the open source new solver rhoCentralRfFoam, previously developed and used here. Secondly, to study the generation of detonation cellular structures using discrete high energy ignition points as perturbation sources.

Reactive Euler equations

Two-dimensional structures of detonation waves can be detected and traced by applying the unsteady Euler equations to rate-controlled chemically active flows.

$$\frac{\partial \mathbf{u}}{\partial t} + \frac{\partial \mathbf{F}}{\partial x_i} = \mathbf{Q} \tag{1}$$

where $\mathbf{u}$, $\mathbf{F}$ and $\mathbf{Q}$ are the conserved variables, their corresponding fluxes and their associated source terms, respectively. Therefore,

$$\mathbf{u} = [\rho, (\rho \mathbf{U}), (\rho E), (\rho Y_i)]^T \tag{2}$$

$$\mathbf{F} = [\rho \mathbf{U}, (\rho \mathbf{U}\mathbf{U} + p), (\rho E \mathbf{U} + \mathbf{U}p), (\rho Y_i \mathbf{U})]^T \tag{3}$$

$$\mathbf{Q} = [0, 0, (\dot{\omega}_T), (\dot{\omega}_i)]^T \tag{4}$$

Given the mass fractions condition, $\sum (Y_k) = 1$, in 2D simulations a set of $N + 3$ transport equations is required in each control volume. It must be noted that the total non-chemical energy used (E) is defined here as:

$$E = h_s - p\rho^{-1} + \frac{1}{2}||\mathbf{U}||^2 \tag{5}$$

and the sensible enthalpy (h_s) is related to temperature T, by

$$h_s = \int_{T_0}^{T} c_p dT \tag{6}$$

The implicit Eq. (6) for temperature is solved using a Newton-Raphson iterative technique. Pressure constant heat capacity (c_p) is a function of temperature and species mass fractions. Therefore, this functional dependence is modeled by computing c_p from

$$c_p = \sum_i^N c_{pi} Y_i \tag{7a}$$

$$c_{pi} = c_{pi}^{\circ} W_i^{-1} \tag{7b}$$

W_i being the molecular weight of species i. The molar constant pressure heat capacities (c_{pi}°) of species are obtained using the JANAF polynomials [37]. The heat capacity ratio (γ) is calculated by:

$$\gamma = \frac{c_p}{c_p - R} \tag{8}$$

where R is the mixture constant ($R = R_u \sum_i^N Y_i W_i^{-1}$). The thermal state equation for a mixture of N ideal gases can be written as:

$$p = \sum_i^N p_i \tag{9}$$

$$= T\rho R_u \sum_i^N Y_i W_i^{-1} \tag{10}$$

The energy equation source term is computed by

$$\dot{\omega}_T = \sum_{k=1}^{N} \dot{\omega}_k \Delta h_{f,k}^{\circ} \tag{11}$$

where $\dot{\omega}_k$ is the production/consumption rate of the species k and $\Delta h_{f,k}^{\circ}$ its formation (chemical) enthalpy. The production/consumption rate of each species is defined by the selected chemical model. Subsequently, the mass rate of any species k by the reaction i is:

$$\omega_{i,k} = \left[\dot{C}_{k,i}\right] W_k \tag{12}$$

$[\dot{C}_{k,i}]$ being its molar rate.

Numerical solution

Governing equations are discretized into the finite volume framework provided by the open source package OpenFOAM®. A generic cell array can be seen in Fig. 1. Although the OpenFOAM® architecture only supports three-dimensional mesh configurations, the package also provides suitable boundary conditions that must be applied to non-considered directions in order to perform one-dimensional, two-dimensional or axisymmetrical simulations. For solutions in 2D, the empty

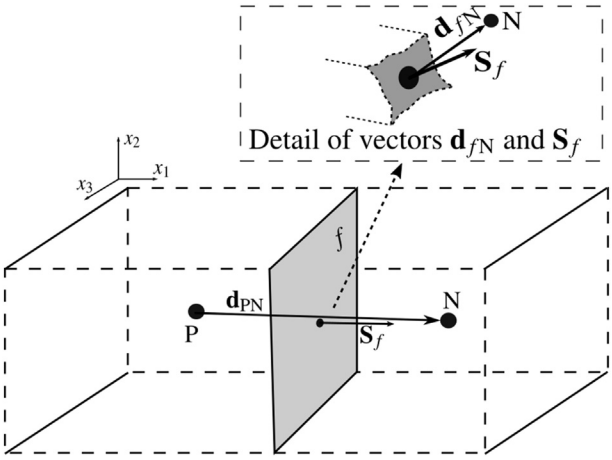

Fig. 1 – Finite volume discretization.

boundary condition is applied in the x_3 direction (Fig. 1). Thus, all equations and terms related to this direction are not taken into consideration [38].

From Fig. 1, the following elements can be identified: $\mathbf{S}_f$, the face area vector, defined as the dot product of the normal unitary vector with its area; $\mathbf{d}_{fN}$ a vector between neighbor cell N and face centroids; $\mathbf{d}_{PN}$ the vector that connects the owner (P) and neighbor (N) cell centroids. The convection-reaction equation for an arbitrary tensorial quantity ψ can be integrated over the control volume (V) for obtaining:

$$\frac{\partial}{\partial t}\int_V \rho\psi dV + \int_s \rho\psi(\mathbf{U}\cdot d\mathbf{S}) = \int_V Q(\psi) dV \tag{13}$$

After approximating the surface integral of the convective term, and the volume integral of the source term, Eq. (13) can be written as:

$$\frac{\partial}{\partial t}\int_V \rho\psi dV + \sum_f \phi_f \psi_f = Q(\psi)_p V_p \tag{14}$$

In this semi-discrete form, the surface integrals can be approximated by a product of the volumetric flux ($\phi_f = \mathbf{U}_f \cdot \mathbf{S}_f$) with a face reconstructed value of ψ_f. It must be noted that the approximation used for the source term integral guarantees second order as well.

Convective and gradient terms computation

To evaluate any convective term, the second order scheme of Kurganov, Noelle, and Petrova (KNP) is selected [31]. The KNP scheme is a Riemann solver free technique that does not involve characteristic information and avoids exact Jacobian evaluations. Therefore, this scheme is an interesting alternative to traditional methods. The physical domain is discretized into Nc cells, in which all thermo-physical and dependent variables are stored at cell centroids (collocated cell arrangement). In the framework provided by OpenFOAM®, Kurganov flux approximations are written as:

$$\phi_f\psi_f = \alpha_+\phi_{f+}\psi_{f+} + \alpha_-\phi_{f-}\psi_{f-} + \omega_f\left(\psi_{f-} - \psi_{f+}\right) \tag{15}$$

Gradient terms are evaluated according to

$$\sum_f \mathbf{S}_f\psi_f = \sum_f \left[\alpha_+\mathbf{S}_f\psi_{f+} + \alpha_-\mathbf{S}_f\psi_{f-}\right] \tag{16}$$

The scheme parameters (ψ_{f+}, ψ_{f-}, α_+, α_-, and ω) are computed following the proposed approach by Greenshields [25]. The numerical procedure involves face reconstruction of dependent variables (T, ρ, p, Y_i, etc). The interpolation procedure uses a limiter to switch between low- and high-order schemes on the basis of a flux limiter function (in this case van Leer, [39]).

Temporal integration

A fractional step approach is used here, followed by solving the chemical problem. Later, the fluid-dynamic equations are integrated over time [40]. Consequently, the overall reactive problem is split into subproblems, described as:

$$\frac{\partial}{\partial t}(\psi) = S(\psi, t) \quad CI : \psi^{n-1}\xrightarrow{\Delta\tau}\widehat{\psi}^{n} \tag{17a}$$

$$\frac{\partial}{\partial t}(\psi) + \mathscr{L}(\psi) = S(\psi, t) \quad CI : \widehat{\psi}^{n}\xrightarrow{\Delta t}\psi^{n} \tag{17b}$$

For solving the ODE system of Eq. (17a), the SIBS method is employed. The SIBS method splits the time step Δt into n sub-steps, and $\Delta\tau$ is determined using a modified midpoint technique [41]. Also, in each one of these sub-steps, system integration is performed. Thereafter, the Aitken-Neville algorithm is used to extrapolate from the sub-step values to the ODE solution, valid at $t + \Delta t$. With these values, new source terms of species and energy are computed, and then, the whole fluid dynamic system is evolved to $t + \Delta t$ (Further details can be found in Ref. [41].).

Boundary conditions

The purpose of all the simulations performed here is to obtain a good visualization of cellular structures that develop in 2D detonations. Therefore, all simulations involve domains like a physical 2D shock tube closed at one end. In order to solve the governing equations over two-dimensional configurations, slip boundary conditions must be imposed on the top and bottom walls, and on the closed end of the tube. Then,

$$\mathbf{U}\cdot\mathbf{n} = 0 \tag{18}$$

$\mathbf{n}$ being the unit normal vector to walls. All other fields at walls must satisfy the zero gradient condition, that is

$$\left.\frac{\partial \mathbf{u}}{\partial \mathbf{n}}\right|_{\delta\Omega} = 0 \tag{19}$$

In order to perform 2D simulations on lateral surfaces, limiting the computational domain, the empty boundary condition is applied.

Chemical kinetic model

To compute source terms in the energy and species transport equations, an appropriate chemical kinetic model for hydrogen oxidation is needed. Any model describing the interaction of M elementary reactions and N species can be written in the compact form as:

$$\sum_{k=1}^{N} \nu_{ki}^{'}[C_k] \xrightarrow{k_i^f} \sum_{k=1}^{N} \nu_{ki}^{''}[C_k] \tag{20}$$

$$\sum_{k=1}^{N} \nu_{ki}^{'}[C_k] \xleftarrow{k_i^b} \sum_{k=1}^{N} \nu_{ki}^{''}[C_k] \tag{21}$$

where $\nu_{ki}^{'}$ and $\nu_{ki}^{''}$ are reactants and products stoichiometric coefficients, k_i^f and k_i^b are forward and backward rates constants of reaction i, and $[C_k]$ the molar concentration of the species k. In terms of mass reaction rates ($\rho Y_k/W_k$ equals the molar concentration of species k, W_k being the molecular mass) the progress rate R_i of reaction i is written as:

$$R_i = k_i^f \prod_{k=1}^{N}\left(\frac{\rho Y_k}{W_k}\right)^{\nu_{ki}^{'}} - k_i^b \prod_{k=1}^{N}\left(\frac{\rho Y_k}{W_k}\right)^{\nu_{ki}^{''}}$$

The backward rates are usually computed from the forward rates through the equilibrium constant [42]. Also, the rate production of species k due to reaction i is subsequently given by

$$\dot{\omega}_{ki} = W_k\alpha_i\left(\nu_{ki}^{''} - \nu_{ki}^{'}\right)R_i$$

Note that to account for third body effects on the rate production R_i of species k, the factor α_i has been introduced. Finally, the total rate $\dot{\omega}_k$ of species k is the sum of rates $\dot{\omega}_{ki}$ produced by all reactions. Therefore,

$$\dot{\omega}_k = \sum_{i=1}^{M} \dot{\omega}_{ki}$$

The chemical system can be represented by a matrix of stoichiometric coefficients with dimensions $N \times M$ in which rows represent species and columns signify reactions. This system involves solving N stiff ODEs in each control volume and each time step. In this work, the chemical process is modeled utilizing the hydrogen-air oxidation mechanism as proposed by Marinov [17], which involves 8 species ($H_2, H, O_2, O, OH, HO_2, H_2O_2, H_2O$) plus N_2 and/or Ar, and 25 reactions (See Table 1). It must be noted that the N_2 is assumed to be an inert species and its contribution to the kinetics is that of a third body. Also, Ar is a diluent, which is assumed to be an inert species as well. In Table 1, all reactions are listed along with the necessary parameters for computing each one of the rates with the Arrhenius formula:

$$k = AT^b\exp\left(\frac{E_a}{RT}\right) \tag{22}$$

Pressure dependence is considered through the Lindemann form [42], which is:

Table 1 – Marinov 1996 chemical kinetic model [units: s, mol, cm^3, cal and K].

Reaction	A	b	Ea
(1) $OH + H_2 \leftrightarrows H + H_2O$	2.14E+08	1.52	3449.0
(2) $O + OH \leftrightarrows O_2 + H$	2.02E+14	−0.4	0.0
(3) $O + H_2 \leftrightarrows OH + H$	5.06E+04	2.67	6290.0
(4) $H + O_2(+M) \leftrightarrows HO_2(+M)$	4.52E+13	0.0	0.0
Low	1.05E+19	−1.257	0.0
(5) $H + O_2(+N_2) \leftrightarrows HO_2(+N_2)$	4.52E+13	0.0	0.0
Low	2.03E+20	−1.59	0.0
(6) $H + O_2(+H_2) \leftrightarrows HO_2(+H_2)$	4.52E+13	0.0	0.0
Low	1.52E+19	−1.133	0.0
(7) $H + O_2(+H_2O) \leftrightarrows HO_2(+H_2O)$	4.52E+13	0.0	0.0
Low	2.10E+23	−2.437	0.0
(8) $OH + HO_2 \leftrightarrows H_2O + O_2$	2.13E+28	−4.827	3500.0
(8b) $OH + HO_2 \leftrightarrows H_2O + O_2$	9.10E+14	0.0	10964.0
(9) $H + HO2 \leftrightarrows OH + OH$	1.50E+14	0.0	1000.0
(10) $H + HO_2 \leftrightarrows H_2 + O_2$	8.45E+11	0.65	1241.0
(11) $H + HO_2 \leftrightarrows O + H_2O$	3.01E+13	0.0	1721.0
(12) $O + HO_2 \leftrightarrows O_2 + OH$	3.25E+13	0.0	0.0
(13) $OH + OH \leftrightarrows O + H_2O$	3.57E+04	2.4	−2112.0
(14) $H + H + M \leftrightarrows H_2 + M$	1.00E+18	−1.0	0.0
(15) $H + H + H_2 \leftrightarrows H_2 + H_2$	9.20E+16	−0.6	0.0
(16) $H + H + H_2O \leftrightarrows H_2 + H_2O$	6.00E+19	−1.25	0.0
(17) $H + OH + M \leftrightarrows H_2O + M$	2.21E+22	−2.0	0.0
(18) $H + O + M \leftrightarrows OH + M$	4.71E+18	−1.0	0.0
(19) $O + O + M \leftrightarrows O_2 + M$	1.89E+13	0.0	−1788.0
(20) $HO_2 + HO_2 \leftrightarrows H_2O_2 + O_2$	4.20E+14	0.0	11982.0
(20a) $HO_2 + HO_2 \leftrightarrows H_2O_2 + O_2$	1.30E+11	0.0	−1629.0
(21) $OH + OH(+M) \leftrightarrows H_2O_2(+M)$	1.24E+14	−0.37	0.0
Low	3.04E+30	−4.63	2049.0
Troe [0.470 100.0 2000.0 1.0E + 15]			
(22) $H_2O_2 + H \leftrightarrows HO_2 + H_2$	1.98E+06	2.0	2435.0
(23) $H_2O_2 + H \leftrightarrows OH + H_2O$	3.07E+13	0.0	4217.0
(24) $H_2O_2 + O \leftrightarrows OH + HO_2$	9.55E+06	2.0	3970.0
(25) $H_2O_2 + OH \leftrightarrows H_2O + HO_2$	2.40E+00	4.042	−2162.0

$$k = k_\infty \left(\frac{P_r}{1+P_r}\right) F \tag{23}$$

P_r being the reduced pressure, related to the concentration of the mixture $[C_M]$ by

$$P_r = \frac{k_0 [C_M]}{k_\infty}$$

where k_∞ is the constant rate at the high-pressure limit, and k_0 the constant rate at the low-pressure limit (keyword: Low in Table 1). In the Lindemann approach, the F function in Eq. (23) is taken as unity and it is applied to reactions R_4, R_5, R_6, R_7. In the method proposed by Troe [42], the function F is expressed as:

$$\log F = \left\{1 + \left[\frac{\log P_r + c}{n - d(\log P_r + c)}\right]^2\right\}^{-1} \log F_{cent}$$

where

$$c = -0.4 - 0.67 \log(F_{cent})$$

$$n = 0.75 - 1.27 \log(F_{cent})$$

$$F_{cent} = (1 - a)\exp(-T/T^{***}) + a\exp(-T/T^{*}) + \exp(-T^{**}/T)$$

The parameters a, T^{***}, T^{*} and T^{**} are specified as inputs on the typical format of CHEMKIN® (keyword Troe in Table 1).

Detonation cellular structure

As Vasil'ev indicates in his review paper [43], transverse waves developed in a confined combustible mixture induce perturbations resulting in a wave front that does not remain planar and shows convex segments and typical Mach's stems bifurcations. These wave interactions are then characterized by triple points whose displacements generate the alleged cellular-pattern.

Detonation cell size is a measure of the mixture reactivity and small cells indicate a more reactive mixture. Consequently, in order to obtain acceptable cell sizes within reasonable computational costs, a hydrogen-oxygen mixture diluted with argon is used. Argon dilution provides a reduction on the mixture reactivity, which enhances cell dimensions [3,44]. The selected stoichiometric hydrogen-oxygen mixture diluted with argon is $2H_2 : O_2 : 7Ar$. Also, when the chemical kinetic model of Marinov [17] is applied to this mixture, it is assumed that the diluent Ar replaces and plays a similar role to N_2 as inert species.

Cellular structures can be naturally formed as a consequence of interacting waves, which are intrinsically dependent on instabilities developed in the flow field. Nevertheless, on numerical simulations, it has been a regular practice to use artificial perturbations to trigger the formation of cellular structures [3,10,45,46]. On early numerical simulations, Gamezo [44] noted that numerical noise could be a source of perturbations for the formation of cellular structures. However, using numerical noise as perturbations can take excessive computational times to induce cellular patterns. Subsequently, artificial perturbation sources have been proposed and tested: unreacted pockets behind the front blast [3,46], internal energy random perturbations [10], sloped initial front [47], several ignition points with high energy [45], and random perturbation of density in the unburned mixture [48]. Several ignition points are further used as perturbation sources and the work of Kirillov [45] has been selected for comparing results with those obtained with rhoCentralRfFoam. It must be noted that the numerical techniques used here and in the work of Kirillov are different, but the underlying kinetic model is the same.

The initial configuration can be seen in Fig. 2, where the adopted labels for nominating each boundary are also indicated. The computational domain has a length of 0.3082 m and is 0.0616 m wide. On the left side, there are three equidistant

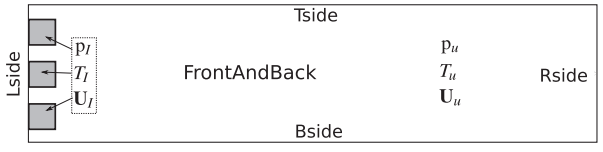

Fig. 2 – Computational domain and initial configuration (Note that FrontAndBack boundary is defined on lateral planes).

Table 2 – Boundary conditions (Zg: zero gradient).

Boundary	p	T	U	Y_i
Tside/Bside	zG	zG	Slip	zG
Lside	zG	zG	Slip	zG
Rside	zG	zG	zG	zG
FrontAndBack	Empty	Empty	Empty	Empty

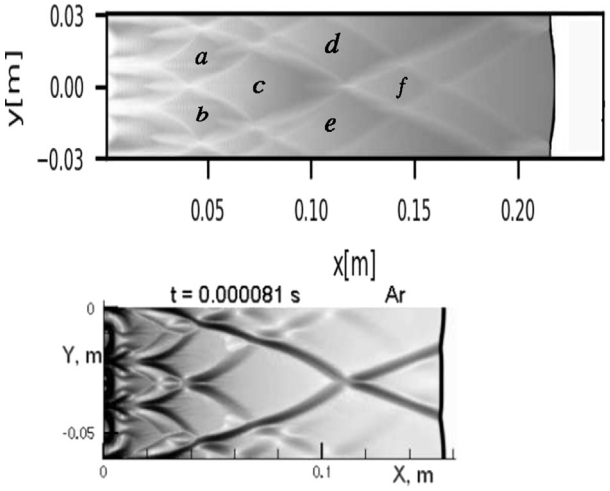

Fig. 3 – Development of cellular structures close to ignition sources (top: rhoCentralRfFoam; bottom: Kirillov).

zones of 3.072 $mm \times 8.8\,mm$, each one identified as a high energy point ($p_I = 1000p_u$, $T_I = 25T_u$, $U_I = 0\ ^m/_s$). They are used to ignite the $2H_2 : O_2 : 7Ar$ fuel mixture. The unburned fuel conditions are: $p_u = 6670$ Pa, $T_u = 298\,K$ and $U_u = 0\ ^m/_s$. Boundary conditions imposed to different regions are summarized in Table 2.

The numerical grid resolution has a direct relation with the induction length and the unburned combustible mixture induction time estimated in $\tau_i \approx 119\mu s$ [23,49]. Subsequently, the induction length becomes $L_i \approx 1.3\,mm$, and a mesh with $\sim 2350 \times 273$ cells in x_1 and x_2 respectively should be used. This results in approximately 10 cells per induction length along x_1 and 6 along x_2. Although it would be recommended to use at least 10 cells per induction length in both x_1 and x_2, the reduction along the x_2 direction is made to limit the computational cost with minimal resolution loss. Indeed, this mesh arrangement provides a resolution of $\sim 0.0296\,mm^2$ with 641550 computational cells. The computation is carried out with the cluster of the National University of Córdoba (UNC) called Mendieta,[1] using a complete node (16 processors). Therefore, the computational domain is decomposed into 16 sub-domains, resulting in almost 40096 cells per processor. Moreover, it takes 54.93 h of computational time to reach a physical simulation time of $103.7\mu s$ assuming a maximum Courant number of 0.1. Fig. 3 shows computed cellular structures near ignition sources using the rhoCentralRfFoam solver, and simultaneously, the cellular structures computed

[1] http://ccad.unc.edu.ar/equipamiento/cluster-mendieta/.

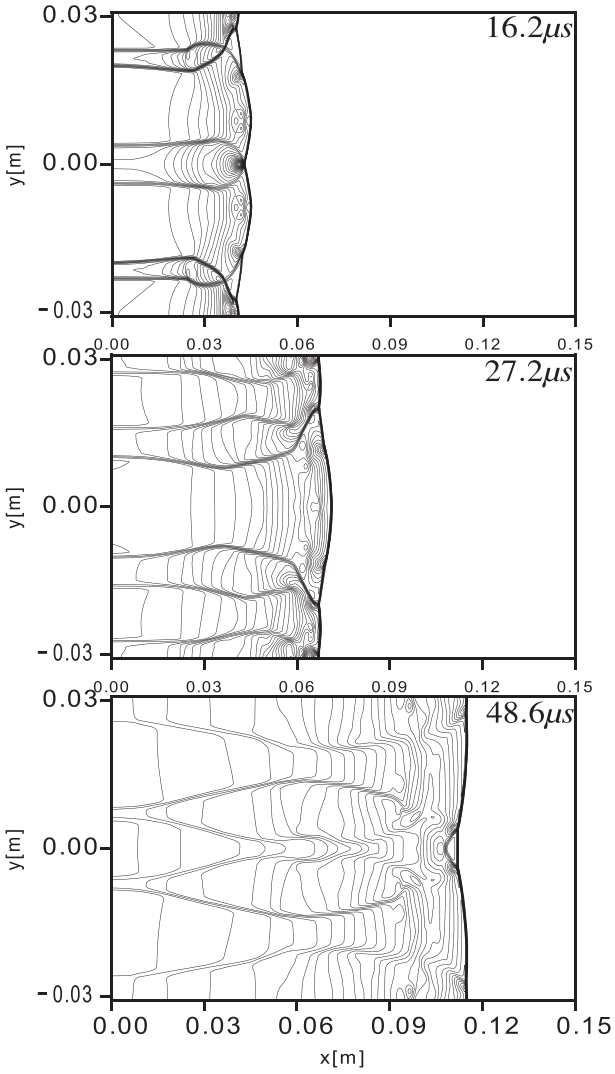

Fig. 4 – Isobaric configurations corresponding to 16.2μs, 27.8μs and 48.6μs.

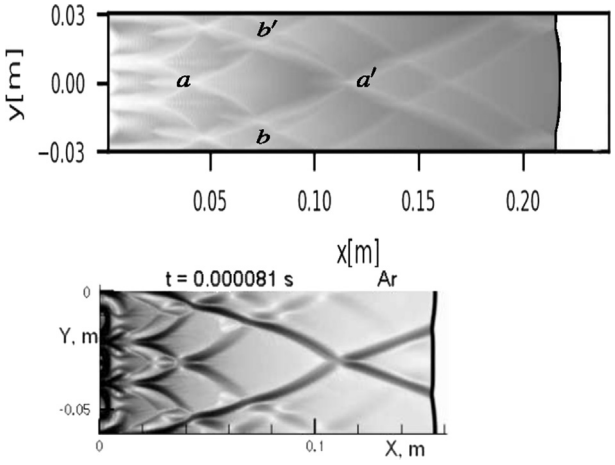

Fig. 5 – Computed motion of triple points describing the formation of cell c.

Table 3 – Comparison of cellular structure dimension for ($2H_2 : O_2 : 7Ar$ $p_u = 6670\ Pa$, $T_u = 298$).

Ref.	α	λ	c^{ar}	Kinetic model
rhoCentralRfFoam	0.074	0.032	0.43	Marinov
Kirillov et al. [45]	0.078	0.033	0.42	Marinov
Eckett [50]	0.054	0.03	0.55	8 species/ 24 reactions
Oran et al. [6]	0.055	0.03	0.54	8 species/ 24 reactions
Lefebvre & Oran [51]	0.077	0.03	0.42	Two steps model
Lefebvre et al. (experimental) [52]	0.17	0.09	0.52	[*smoke foil*]

by Kirillov [45]. At first glance, there are similarities between computed waves and their interactions in both cases. A well-shaped early cellular structure c can be identified, as well as other structures surrounding it (not so clearly defined). The later are nominated *a*, *b*, *d* and *e*. Furthermore, $x \sim 0.12\ m$, the onset of a new cellular pattern is detected. In Fig. 4, computed isobaric contours taken from the field region of Fig. 3 at 16.2μs, 27.8μs and 48.6μs are presented. The first configuration depicts the triple point that defines the start vertex a of the early cell *c*, the second (t = 27.8μs) shows two triple points that define vertices *b* and *b'* (Fig. 5) also in the early cell, and the last depicts the motion and convergence of triple points to the center line, defining the vertex *a'* that closes the cell *c*. In Fig. 5, the vertices (a, a', b, b') of cell *c* are shown, and the cell characteristic dimensions are defined as:

$\{a, a'\} \rightarrow \alpha = 0.074\ m$

$\{b, b'\} \rightarrow \lambda = 0.032\ m$

In Table 3, the obtained cell *c* values of α and λ and their corresponding aspect ratio $c_{ar} = \lambda/\alpha$, are listed. In addition, the appropriate reference data for comparison are also included. There are acceptable agreements when compared with Kirillov results, probably because both studies used the same kinetic model (Marinov [17]). Moreover, detonation starting conditions for both studies are also the same. However, when compared with others results [6] and [50], significant differences were detected. Also, the data provided by Lefebvre and Oran [51] is considered exceptional, since they used a highly simplified kinetic model (only two steps). The Lefebvre experimental data obtained with the smoke foil technique presents an aspect ratio value close to those given in Refs. [50] and [6]. As regards to discrepancies shown in Table 3, the question is if a cellular structure like *c* built in the neighborhood of discrete but strong ignition sources, is conserved when the computational domain is extended along the x-axis. To answer this question, the previous computational domain was extended to 0.5*m*, and then a new calculation was made. To guarantee proper resolution, a mesh of $\sim 10^6$ cells are employed. Subsequent to 350μs of physical time simulation, the cellular structure shown in Fig. 6 a develops and an experimental well-formed cellular structure is shown for comparison in Fig. 6 b [52]. At the initial stages, the previous results are reproduced (see Fig. 3). However, cells obtained for $x > 0.25m$ are larger than early cells (mainly, than cell *c*). These new cells now have $a \sim 0.13m$ of length (almost 100 times greater than $L_i = 0.0013m$), and the aspect ratio becomes closer to 0.48. This aspect ratio compares better with data presented in

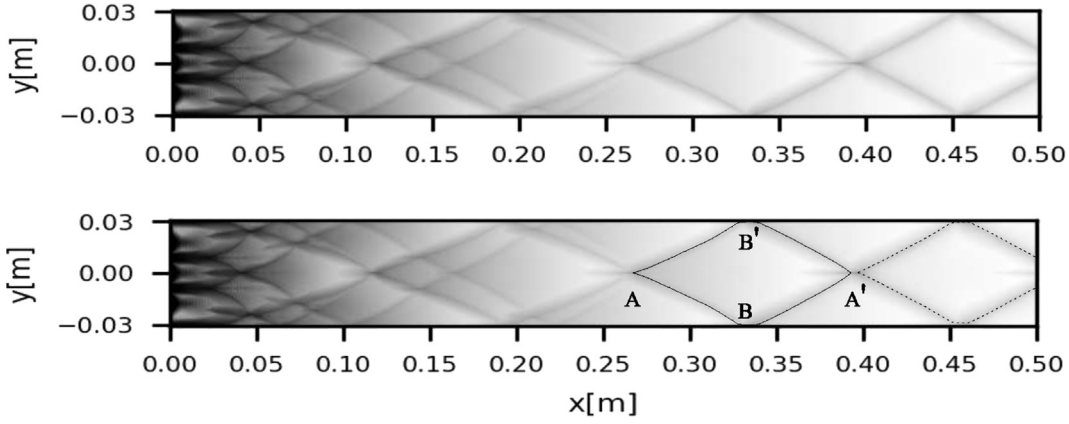

(a) rhoCentralRfFoam computation (numerical *schlieren* of max(p))

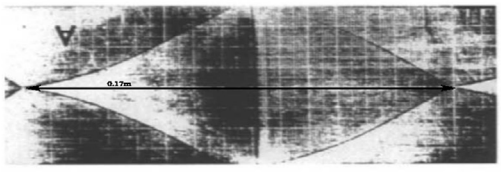

(b) Experimental observation

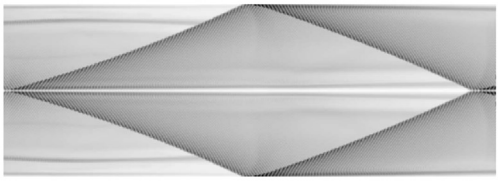

(c) rhoCentralRfFoam detail (numerical *schlieren* of max(|ω|))

Fig. 6 – Development of the cellular structure at t = 350μs.

Table 3. It is interesting to note that the cell's aspect ratio obtained here for $x > 0.25\ m$, tends to be in good agreement with the computations of the others authors, even with distinct kinetic models and geometries (Fig. 7).

With the purpose of improving results presentation from numerical simulations, a way of numerically emulating the *schlieren* technique is implemented [53]:

$$S_h = h_1 \exp\left(h_2 \frac{|\nabla f|}{|\nabla f|_{max}}\right) \tag{24}$$

where h_1 and h_2 are properly selected constants and f the field variable used for visualization (usually density, pressure or vorticity). Fig. 8 a built after 81.6μs of real-time using density contours provided by a numerical *schlieren*, shows transverse

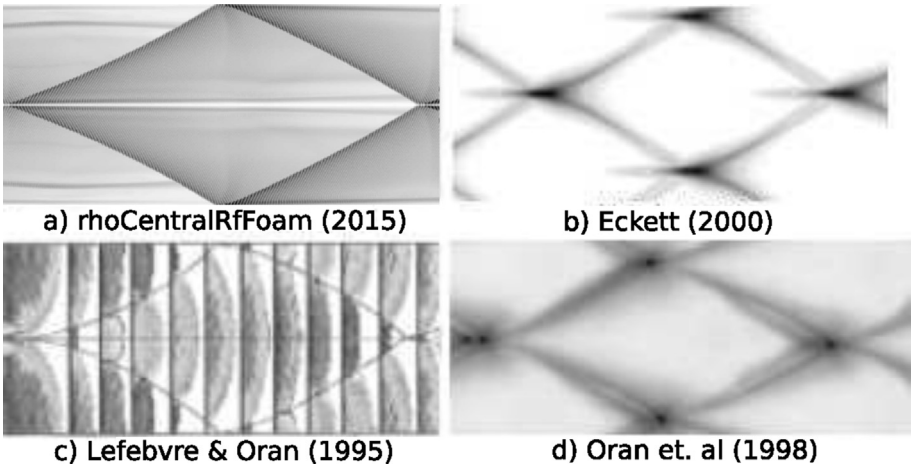

Fig. 7 – Comparison of cellular structure configurations.

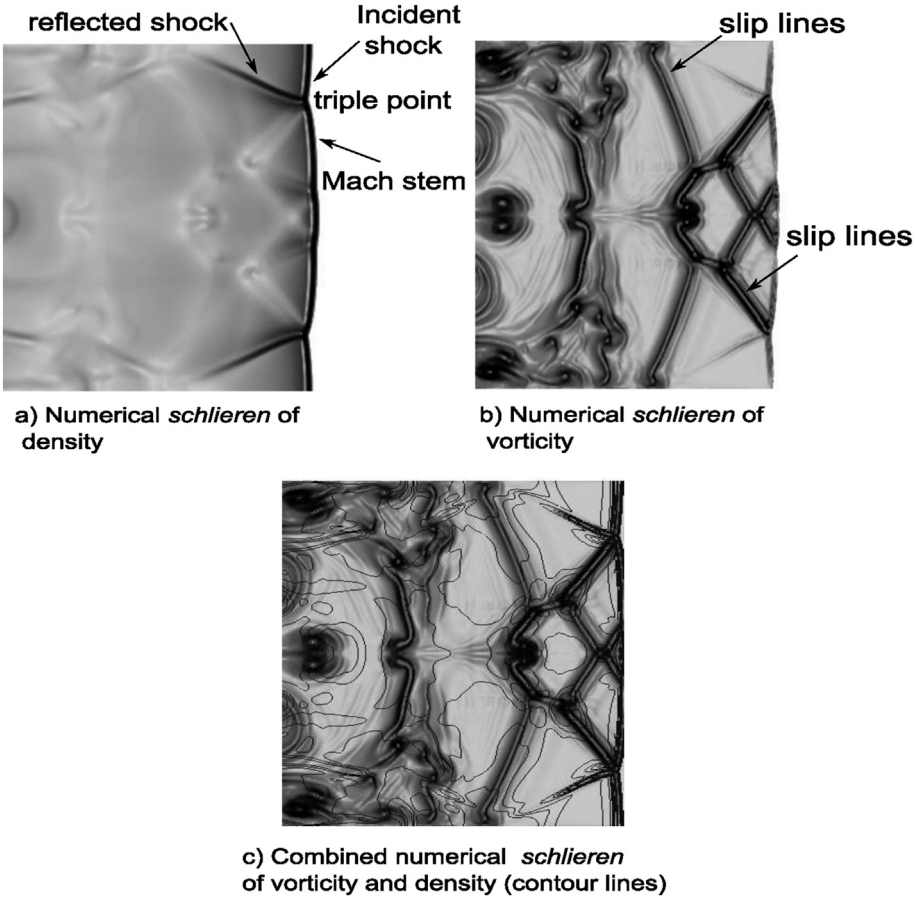

Fig. 8 – Wave interactions at triple points ($t = 81.6\mu s$).

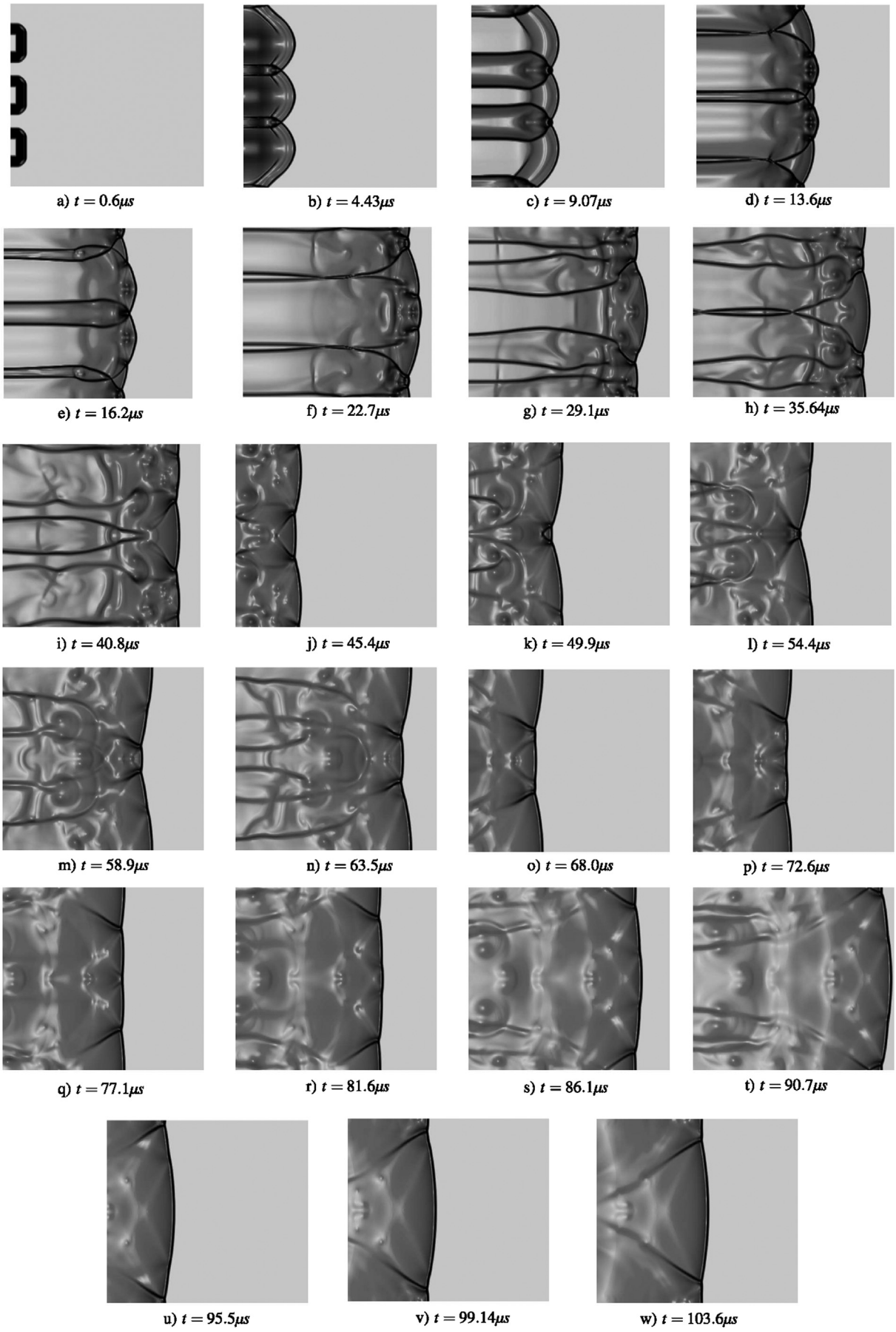

Fig. 9 – Cellular structure formation process: Evolution of triple points.

waves interacting with the detonation front. These interactions perturb the detonation front and generate configurations like irregular reflections. Also, the transverse wave takes the reflected wave role, the front is bifurcated and subsequently the incident shock and the Mach stem are defined. Slip lines are properly identified and represented, by means of the numerical *schlieren* of vorticity and combined vorticity-density. At this time $(81.6\mu s)$ it is evident that the detonation front has been strongly disturbed by the used ignition technique (Fig. 8b and c). However, these highly perturbed structures disappear when the wave front reaches $x \approx 0.215m$ and the configurations shown in Figs. 6 and 7 remain. It is noteworthy that at $x \approx 0.17m$ the pressure jump across the front is 34.78 and at $x \approx 0.215m$, it is 27.05, which are values of a typical overdriven detonation. When the front approximates $0.47m$, the pressure jump is 23.14 and the detonation velocity is about 10% higher than the Chapman-Jouguet equilibrium value [54]. Thereafter regular cell patterns are obtained.

In Fig. 9 a succession of *schlieren* pictures is presented. They describe the formation of triple points and how its displacement defines a cellular structure as time goes by. At $t = 13.6\ \mu s$ (Fig. 9-d), perturbations are detected that alter the wave front. Successively, at $t = 22.7\ \mu s$ (Fig. 9-f), it is observed that triple points are formed as a consequence of multiple secondary shocks, which interact with the detonation front. At $t = 54.4\ \mu s$, the buildup (Fig. 9-l) of the triple point located at the front wave center (see Fig. 4) is completed. From $54\mu s$ to $103.6\mu s$, it is indicated how the duct width is limiting the vertical motion of triple points and of course, its influence on the process of cellular structure formation.

Conclusions and future work

This work verifies the ability of the rhoCentralRfFoam solver to deal with detonations cellular structures in 2D chemically reacting flows, and thus it also confirms the efficiency of the used KNP scheme. Results obtained with a $2H_2 : O_2 : Ar$ combustible mixture, have shown good correlation with the available experimental data. Computed isobaric contours have demonstrated how the motion of triple points defines cellular structures formed close to ignition points. However, these structures are in a transitional state, and if the calculation domain is extended, a unique steady cellular pattern different from the initial configuration develops. It can be said; it becomes independent of the initial perturbations. The aspect ratio of this constant shape tends to agree better with available data. It is worth noting that for achieving this steady state shape, it was necessary to work with an expanded domain ($\sim 65\%$ greater and having ~ 1000000 cells). For tracking the evolution of cellular structures towards the last steady configuration, after implementing a numerical *schlieren* procedure, a series of pictures covering $104\mu s$ of flow real-time is presented.

Detonation cellular patterns are classified as having either a regular or an irregular structure. In this work, detonation cellular structures related to hydrogen-oxygen fuel mixtures were considered. These mixtures have low activation energies and are associated with regular cellular patterns, which are properly predicted only considering ignition by adiabatic shock compression and without accounting for any transport mechanism [55].

Mixtures of hydrocarbon fuels with oxygen or air, exhibit detonations with much more stochastic-looking cell structures: cells size is variable, the wave front can be highly turbulent, and often give rise to unburned pockets in its wake [8]. These unburned pockets burn through turbulent mixing with combustion product gases and not by shock compression alone, then to get further insight into detonation propagation in hydrocarbon fuel mixtures it is essential to model ignition with both, turbulent mixing and compression. For treating simultaneously, turbulent mixing and combustion rates in mixtures prone to irregular structures, it should be preferred numerical simulations based on LES strategies.

A moving-adaptive mesh will also be implemented in order to reduce mesh size, thus decreasing the amount of computations. In this context, the approach to be used will be that of [56]. This methodology shall be useful for defining the number of cells locally needed around places of interest (e.g. detonation fronts, triple points, strong chemical activity, and of unburned pockets).

Acknowledgements

This work was supported by CONICET, SECyT-UNC and MCyT Córdoba. The authors also would like to thank Dr. Andrés Cimino for his helpful and constructive comments that greatly contributed to improving the final version of the paper.

REFERENCES

[1] Lee JH. The detonation phenomenon. Cambridge University Press; 2014.
[2] Zhang B, Kamenskihs V, Ng HD, Lee JH. Direct blast initiation of spherical gaseous detonations in highly argon diluted mixtures. Proc Combust Inst 2011;33(2):2265–71.
[3] Oran ES, Weber JW, Stefaniw EI, Lefebvre MH, Anderson JD. A numerical study of a two-dimensional H_2-O_2-Ar detonation using a detailed chemical reaction model. Combust Flame 1998;113(1–2):147–63. http://dx.doi.org/10.1016/S0010-2180(97)00218-6.
[4] Quirk JJ. Godunov-type schemes applied to detonation flows. Springer; 1994.
[5] Ning J, Zhao H, Li J, Ma T, Ren H. Numerical simulation of H_2–O_2 gaseous detonation on the wedge. Int J Hydrogen Energy 2015;40(37):12897–904.
[6] Oran ES, Weber JW, Stefaniw EI, Lefebvre MH, Anderson JD. A numerical study of a two-dimensional H_2-O_2-Ar detonation using a detailed chemical reaction model. Combust Flame 1998;113(1):147–63. http://dx.doi.org/10.1016/S0010-2180(97)00218-6.
[7] Deiterding R. Parallel adaptive simulation of multi-dimensional detonation structures. Ph.D. thesis. Brandenburgischen Technischen Universität Cottbus; 2003.
[8] Maxwell BM, Bhattacharjee RR, Lau-Chapdelaine SS, Falle SA, Sharpe GJ, Radulescu MI. Influence of turbulent fluctuations on detonation propagation. J Fluid Mech 2017;818:646–96.
[9] Sharpe GJ. The effect of curvature on detonation waves in type ia supernovae. Mon Not R Astron Soc 2001;322(3):614–24.

[10] Hu X, Khoo B, Zhang D, Jiang Z. The cellular structure of a two-dimensional H_2/O_2 detonation wave. Combust Theory Model 2004;8(2):339–59.

[11] Geßner T. Dynamic mesh adaption for supersonic combustion waves modeled with detailed reaction mechanisms. Ph.D. thesis. Albert Ludwigs Universit at Freiburg im Breisgau; 2001.

[12] Huang W, Wang Z-g, Li S-b, Liu W-d. Influences of H_2O mass fraction and chemical kinetics mechanism on the turbulent diffusion combustion of H_2–O_2 in supersonic flows. Acta Astronaut 2012;76:51–9.

[13] Gutiérrez Marcantoni LF, Tamagno JP, Elaskar SA. RANS simulation of tubulent difussive combustion using OpenFOAM®. J Appl Fluid Mech 2016;9(2):669–82. http://jafmonline.net.

[14] Huang W, Yan L. Numerical investigation on the ram–scram transition mechanism in a strut-based dual-mode scramjet combustor. Int J Hydrogen Energy 2016;41(8):4799–807.

[15] Jachimowski CJ. An analytical study of the hydrogen-air reaction mechanism with application to scramjet combustion. Vol. 2791, National Aeronautics and Space Administration, Scientific and Technical Information Division. 1988.

[16] Jachimowski CJ. An analysis of combustion studies in shock expansion tunnels and reflected shock tunnels. Vol. 3224, National Aeronautics and Space Administration, Scientific and Technical Information Division. 1992.

[17] Marinov N, Westbrook C, Pitz W. Detailed and global chemical kinetics model for hydrogen-air. Vol. 8 of International Symposium on Transport Properties, Lawrence Livermore National Laboratory. 1996. p. 118.

[18] Tamagno JP, Elaskar SA, García JO. A numerical study of planar detonations. Lat Am Appl Res 2012;42(2):161–6.

[19] Tamagno JP, Elaskar SA, Rıos GA. Numerical simulation of time-dependent reacting flows in pulse facilities. Appl Numer Math 2003;47(3–4):515–30.

[20] Wilson G. Time-dependent quasi-one-dimensional simulations of high enthalpy pulse facilities. Arch Set 1963;484(1). http://dx.doi.org/10.2514/6.1992-5096.

[21] Yee HC. A class of high-resolution explicit and implicit shock-capturing methods. Tech rep. 1994.

[22] Kee RJ, Rupley FM, Miller JA. Chemkin-II: a Fortran chemical kinetics package for the analysis of gas-phase chemical kinetics. Tech rep. Livermore, CA (USA): Sandia National Labs; 1989.

[23] Gutiérrez Marcantoni LF, Tamagno J, Elaskar S. rhoCentralRfFoam: an OpenFOAM® solver for high speed chemically active flows –Simulation of planar detonations–. Comput Phys Commun 2017;219:209–22. http://dx.doi.org/10.1016/j.cpc.2017.05.021.

[24] Gutiérrez Marcantoni LF. Simulación numérica de procesos reactivos en mezclas de gases con múltiples componentes. Ph.D. thesis. Universidad Nacional de Córdoba; 2016.

[25] Greenshields CJ, Weller HG, Gasparini L, Reese JM. Implementation of semi-discrete, non-staggered central schemes in a colocated, polyhedral, finite volume framework, for high-speed viscous flows. Int J Numer Methods Fluids 2010;63(1):1–21.

[26] Gutiérrez Marcantoni LF, Tamagno JP, Elaskar SA. High speed flow simulation using OpenFOAM®. In: Cardona A, Kohan HP, Quinterios DR, Storti M, editors. Mecánica Computacional, vol. 31; 2012. p. 2939–59.

[27] Bansal A, Feldick A, Modest M. Simulation of hypersonic flow and radiation over a mars reentry vehicle using OpenFOAM®. In: 50th AIAA aerosp. sci. meeting including the new horizons forum and aerospace exposition; 2012. p. 650.

[28] Casseau V, Scanlon TJ, Brown RE. Development of a two-temperature open-source CFD model for hypersonic reacting flows. In: 20th AIAA int. Sp. Planes hypersonic syst. technol. conf. (July); 2015. p. 1–14. http://dx.doi.org/10.2514/6.2015-3637.

[29] Casseau V, Palharini RC, Scanlon TJ, Brown RE. A two-temperature open-source cfd model for hypersonic reacting flows, part one: zero-dimensional analysis. Aerospace 2016;3(4):34.

[30] Casseau V, Espinoza DE, Scanlon TJ, Brown RE. A two-temperature open-source cfd model for hypersonic reacting flows, part two: multi-dimensional analysis. Aerospace 2016;3(4):45.

[31] Kurganov A, Noelle S, Petrova G. Semidiscrete central-upwind schemes for hyperbolic conservation laws and hamilton–jacobi equations. SIAM J Sci Comput 2001;23(3):707–40. http://dx.doi.org/10.1137/S1064827500373413.

[32] Christov I, Popov B. New non-oscillatory central schemes on unstructured triangulations for hyperbolic systems of conservation laws. J Comput Phys 2008;227(11):5736–57. http://dx.doi.org/10.1016/j.jcp.2008.02.007.

[33] Jiang G-S, Levy D, Lin C-T, Osher S, Tadmor E. High-resolution nonoscillatory central schemes with nonstaggered grids for hyperbolic conservation laws. SIAM J Numer Anal 1998;35(6):2147–68.

[34] Kurganov A, Tadmor E. Solution of two-dimensional Riemann problems for gas dynamics without Riemann problem solvers. Numer Methods Partial Differ Equat 2002;18(5):584–608.

[35] Rinaldi E, Pecnik R, Colonna P. Exact Jacobians for implicit Navier–stokes simulations of equilibrium real gas flows. J Comput Phys 2014;270:459–77.

[36] Touma R, Zeidan D, Habre S. Central finite volume schemes on nonuniform grids and applications. Appl Math Comput 2015;262:15–30.

[37] Stull DR, Prophet H. JANAF Thermochemical Tables. US National Bureau of Standards; 1971.

[38] Jasak H, Jemcov A, Tukovic Z. OpenFOAM: a C ++ library for complex physics simulations. In: Int. work. coupled methods numer. Dyn., vol. 1000, IUC Dubrovnik, Croatia; 2007. p. 1–20.

[39] Van Leer B. Towards the ultimate conservative difference scheme. ii. monotonicity and conservation combined in a second-order scheme. J Comput Phys 1974;14(4):361–70.

[40] Yanenko NN. The method of fractional steps. Berlin, Heidelberg: Springer Berlin Heidelberg; 1971.

[41] Bader G, Deuflhard P. A semi-implicit mid-point rule for stiff systems of ordinary differential equations. Number Math 1983;41:373–98.

[42] Kuo KK. Principles of combustion. 2nd ed. John Wiley & Sons, Inc; 2005.

[43] Vasil'ev AA. Cellular structures of a multifront detonation wave and initiation (review). Combust Explos Shock Waves 2015;51(1):1–20.

[44] Gamezo VN, Desbordes D, Oran ES. Formation and evolution of two-dimensional cellular detonations. Combust Flame 1999;116(1):154–65.

[45] Kirillov I, Strelkova M, Panasenko A, Roekaerts D. Sensitivity to detonation and detonation cellular structure of H_2–O_2–air–H_2–O_2 gas mixtures. In: First int. Conference on hydrogen safety, Pisa, Italy; 2005. p. 8–10.

[46] Kailasanath K, Oran E, Borin J, Young T. A computational method for determining detonation cell size. In: 23rd aerospace sciences meeting; 1985. p. 236.

[47] Choi J, Ma F, Yang V. Some numerical issues on simulation of detonation cell structures. Combust Explos Shock Waves 2008;44(5):560–78.

[48] Short M, Kiyanda CB, Quirk JJ, Sharpe GJ. The role of cellular structure on increasing the detonability limits of three-step

chain-branching detonations. Tech rep. Los Alamos National Laboratory (LANL); 2011.
[49] Chung KL. Combustion physics, vol. 14. Cambridge University press; 2010.
[50] Eckett CA. Numerical and analytical studies of the dynamics of gaseous detonations. Ph.D. thesis. 2000.
[51] Lefebvre M, Oran E. Analysis of the shock structures in a regular detonation. Shock Waves 1995;4(5):277–83.
[52] Lefebvre MH, Weber JW, Oran ES. Numerical simulations of a marginal detonation: wave velocities and transverse wave structure. In: IUTAM symp. on combust. in supersonic flows. Springer; 1997. p. 347–58.
[53] Yates LA. Interferograms, schlieren, and shadowgraphs constructed from real-and ideal-gas, two-and three-dimensional computed flowfields. NASA. Ames Research Center, Technical Paper Contest for Women 1992. Space Challenges: Earth and Beyond. 1993. p. 207–18.
[54] Gordon S, McBride BJ. Computer program for calculation of complex chemical equilibrium compositions and applications. Vol. 1, National Aeronautics and Space Administration, Office of Management, Scientific and Technical Information Program. 1994.
[55] Radulescu M, Sharpe G, Lee J, Kiyanda C, Higgins A, Hanson R. The ignition mechanism in irregular structure gaseous detonations. Proc Combust Inst 2005;30(2):1859–67.
[56] Espinoza DE, Scanlon TJ, Brown RE. Validation of tools to accelerate high-speed cfd simulations using OpenFOAM®. In: 20th AIAA int. space planes and hypersonic systems and technologies conference; 2015. p. 3566.